Nyman, Leo; Frolec, Jiří; Pudas, Marko; Králík, Tomáš; Musilová, Věra; Kallio, Esa

Low-emittance copper-coating system using atomic-layer-deposited aluminum oxide

Published in:
Thin Solid Films

DOI:
10.1016/j.tsf.2022.139179

Published: 01/01/2022

Document Version
Publisher's PDF, also known as Version of record

Please cite the original version:
Nyman, L., Frolec, J., Pudas, M., Králík, T., Musilová, V., & Kallio, E. (2022). Low-emittance copper-coating system using atomic-layer-deposited aluminum oxide. *Thin Solid Films*, *749*, Article 139179. https://doi.org/10.1016/j.tsf.2022.139179

Thin Solid Films 749 (2022) 139179

Contents lists available at ScienceDirect

Thin Solid Films

journal homepage: www.elsevier.com/locate/tsf

Low-emittance copper-coating system using atomic-layer-deposited aluminum oxide

Leo Nyman [a,*], Jiří Frolec [b], Marko Pudas [c], Tomáš Králík [b], Věra Musilová [b], Esa Kallio [a]

[a] School of Electrical Engineering. Aalto University, FI-00076 Aalto, Finland
[b] Institute of Scientific Instruments of the Czech Academy of Sciences. Kralovopolska 147, 612 00 Brno, Czech Republic
[c] Picosun Oy, Masalantie 365, FI-02430 Masala, Finland

ARTICLE INFO

Keywords:
Atomic layer deposition
Nanophotonics
Emissivity
Cryogenics
Spacecraft
Copper

ABSTRACT

Copper, due to its unique properties, has a huge technological importance to our society. However, the oxidation of copper remains an issue in numerous application areas. This is especially the case in visible and IR-band optics, where even minuscule oxide layers degrade the thermo-optical properties of copper surfaces. A solution possibly resides in the application of protective coatings, which can simultaneously impair the low thermal emittance of bare copper surfaces. The present paper examines the use of thin Al_2O_3 layers as a protective coating for copper. Al_2O_3 layers with thickness of 4.5, 9.1, 18.5 or 28.3 nm were deposited on polished copper discs using atomic layer deposition (ALD). The total hemispherical emissivity and absorptivity of these coated copper discs were measured from 20 K up to room temperature. The emissivity and absorptivity of the copper with ALD-deposited Al_2O_3 layers increased with rising temperature and layer thickness. Nonetheless, the observed values stayed below 1.8%, allowing the use of the coated copper in systems where low emission or absorption of thermal radiation is needed. Alongside the experiments, we present a computer-based analysis and interpretation, which may be generally applied for prediction of temperature-dependent emittance of metallic surfaces coated with a thin polar dielectric layer.

1. Introduction

Solid surfaces with low thermal emittance (low-*e*) are a fundamental technology of thermal shielding for space- and cryotechnologies [1,22]. Interestingly, application of this technology to the thermal shields used in the ITER fusion reactor is currently an active research topic [2–4]. One specific example of space applications is the MiniPINS moon mission by the Finnish Meteorological Institute [21]. A low-*e* surface withstanding temperatures down to -170 °C would reduce the power requirements of its heaters. The James Webb Space Telescope (JWST) provides another mission example where thermal radiation is critical [22,23]. Considering telescopes in general, silver is a common reflector material used in primary mirrors. In addition to silver, copper and gold could be used to build high-performance reflectors for terrestrial and space-based IR telescopes [24]. However, both Ag and Cu require the use of protective coatings. A more common use case for this technology can be found in cryostats. Copper is often used as the material of choice for cryostat components [5], securing its place as a common low-*e* surface material. However, oxidation and other forms of chemical reactivity affecting copper remains an issue, as these increase the thermal emittance of the surface in question.

1.1. Low-e surface

Radiative heat transfer takes place between two surfaces through emission and absorption of thermal radiation [7]. For space- and cryotechnologies, the relevant thermal emittance band of electromagnetic radiation typically starts from a few micrometers in wavelength and spans to hundreds of micrometers (from infrared to far infrared radiation). When aiming for a low absorption or emission of thermal radiation, one would normally choose a metal with a good electrical conductivity. It has been shown that low thermal emission is related to the low electrical resistivity of metal. This phenomenon, known as the Hagen–Rubens relation [7,8], gives evidence of the interaction of thermal radiation with free electrons in metals.

The physical model enabling calculation of the infrared optical properties of metals, including their thermal emittance, is Drude's model [7,9,10] which may be justified if the normal skin effect takes

* Corresponding author.
E-mail address: leo.nyman@aalto.fi (L. Nyman).

https://doi.org/10.1016/j.tsf.2022.139179
Received 25 August 2021; Received in revised form 17 February 2022; Accepted 15 March 2022
Available online 16 March 2022

place. The Hagen–Rubens relation is based on a long-wavelength approximation and, therefore, does not hold for all wavelengths covered by the Drude model. In the case of highly conducting metals, such as pure Cu, Au, Ag, Al, we encounter an anomalous skin effect (ASE). The ASE was solved theoretically by Reuter and Sondheimer [11] and the theory was many times revisited and refined from various aspects [12]. Due to the mathematical complexity of the ASE theory, Domoto et al. [13] applied an approximate ASE formula of Dingle [14] for the calculation of optical constants and then the emittance of copper at cryogenic temperatures. Both models, Drude and Dingle, presume knowledge of the direct current (DC) resistivity of the metal in the skin depth of electromagnetic radiation. The ASE theory, unlike the Drude model, explains an important experimental fact as follows. The decrease in emittance with decreasing resistivity (increasing metal purity) is limited to a certain lowest value. In practice, we have seen decreased emissivity with the increase in the purity of copper up to a figure of approximately 99.5 wt% Cu [15]. The use of copper with higher purity has a negligible effect on the emissivity of the surface.

In general, a metal surface is covered with a dielectric layer, which originates from environmental contamination or is created artificially as a chemical barrier. Contrary to metals, polar insulating materials such as inorganic compounds, absorb and emit infrared radiation via the optical modes of atomic lattice vibrations. Infrared absorption of a thin layer of polar dielectrics was studied and estimated in an optical experiment by Berreman [16,17] and later applied in measurement techniques or interpreted in [18,19,20], to give some examples. The Berreman analytical approach [16] shows that a thin layer of polar dielectric on a highly reflective metal does not absorb infrared radiation at the normal angle of incidence.

1.2. Bulk copper as a substrate

Besides the possibility to achieve very low values of emissivity and absorptivity [25,26], other advantageous features of copper are its high thermal and electrical conductivity and excellent solderability. Its main disadvantage resides in its high chemical reactivity, often requiring application of protective coatings. A bulk copper surface is vulnerable to oxidation [27,28,29]. The thickness of this oxide layer is affected by various factors. An approximately 100-nm thick oxide layer was formed on bulk Cu exposed to ambient air at 240 °C for 20 min [27]. At room temperature and below, the Cu-oxide layer thickness typically remains at or below 10 nm [28]. This reactive nature of copper has limited its use in spacecraft external surfaces. Raikar et al. [30] detected the formation of a 55-nm thick Cu_2O layer on copper, after it had been exposed to the space environment for 69 months. This process, which degrades the thermo-optical properties and surface conductivity of a copper surface, is caused by the abundant atomic oxygen in the low-Earth orbits. Accordingly, the European Cooperation for Space Standardization (ECSS) standard ECSS-Q-ST-70–71C (*Materials, processes and their data selection*) prohibits the use of copper coatings on spacecraft external surfaces exposed to atomic oxygen in the low-Earth orbit [31].

1.3. Protecting copper and its alloys

A common solution to prevent oxidation is to apply a barrier coating, to isolate the Cu atoms from oxygen. Such a barrier film needs to withstand the challenges of the operating environment, while preserving the low-*e* nature of polished copper. Therefore, finding an ultra-thin and robust barrier coating for Cu is of critical importance.

Atomic layer deposition (ALD) is a chemical vapor-based coating method that produces ultra-thin films of high uniformity and conformity down to the nanometer range. This process was introduced in the 1970s and initially named “atomic layer epitaxy” [32]. ALD is based on surface-controlled and self-saturating adsorption reactions between the surface and gaseous precursors. The film growth proceeds by sequential atomic layers, which inherently leads to precise control of both film thickness and its chemical composition. Since the reactions by gaseous precursors take place in a vacuum, ALD can deposit extremely conformal coatings on high-aspect-ratio components. ALD Al_2O_3 has been used in the microelectronics industry as a barrier coating (see e.g. [33] and [34]). It has also been shown to improve the corrosion resistance of pure copper surfaces [35]. ALD Al_2O_3 nucleation and growth on copper has been measured by Abdulagatov et al. [36].

The good performance of a vacuum-evaporated Al_2O_3 thin-film coating in space was demonstrated for a silver substrate [37]. Al_2O_3 thin-film coatings, produced with various methods including ALD, have been proposed for use in future space missions for protecting metallic substrates [38].

This article presents the effect of a thin Al_2O_3 layer on the thermal emissivity and absorptivity of a pure copper substrate at cryogenic temperatures. Sections 2.1.–2.4 describe the preparation of the samples with the Al_2O_3 layer, and the technique of emissivity and absorptivity measurements. In Section 2.5 we model the layer effect on thermal radiative properties. We use the published optical constants of Al_2O_3 prepared with different technologies to find out the influence of temperature and Al_2O_3 structure on the studied emissivity and absorptivity of coated copper. In addition, we compare the modelled spectral directional absorptivity with Berreman’s analytic approach. Experimental results are summarized in Section 3. The discussion on possible applications of the low-*e* system studied here (Section 4) is followed by the conclusions which are given in Section 5.

2. Experimental details

2.1. Characteristics of low-e systems

The zenith angle θ (Fig. 1) categorizes the measurements into the two most common characteristics: (a) ε_H (T_R) (the total hemispherical emissivity), which is the total power radiated by a solid surface into a hemisphere divided by the total power radiated by a blackbody under identical conditions; and (b) ε_N (T_R) (the total normal emissivity), which is the case when $\theta < 15°$. The values of ε_H and ε_N differ mutually within the range of approximately 30% where typically $\varepsilon_H > \varepsilon_N$ for metals and the opposite is true for dielectrics [7], $\varepsilon_H < \varepsilon_N$. Analogically, the same is valid for the absorptivities.

Throughout this study, we measure the total hemispherical values ε_H, α_H as characteristics of a low-emissivity system. For interpretation of the measurement results, Section 2.5 presents the calculations of ε_H and α_H based on using optical constants of respective materials in the primary evaluation of spectral directional absorptivity $\alpha(T_S, \lambda, \theta)$ of a smooth planar isotropic surface.

2.2. Samples

The samples (Table 1) were fabricated from a rod of technically pure copper (purity 99.9%, residual-resistivity ratio about 65). Each of these

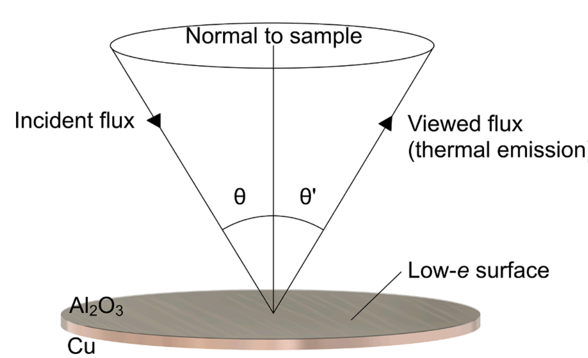

Fig. 1. Illustration of a copper-disk sample (as used in this work), having a thin-film ALD Al_2O_3 coating.

Table 1
List of the measured samples, corresponding layers, and measurements of emissivities and absorptivities.

Sample number	Emissivity measurement (bare Cu)[a]	Absorptivity measurement (bare Cu)[a]	Thickness of ALD coating [nm]	Number of ALD cycles[b]	Emissivity measurement (coated Cu)	Absorptivity measurement (coated Cu)
01	E01u	A01u	4.5	49	E01c	A01c
02	E02u	A02u	9.1	93	E02c	A02c
03	E03u	A03u	18.5	186	E03c	A03c
04	E04u	A04u	28.3	279	E04c	A04c

[a] Each measurement designation starts with "E" or "A" abbreviating the type of measurement (Emissivity or Absorptivity), followed by sample number and ends with the letter "c" (coated by ALD) or "u" (uncoated, i.e. bare Cu).
[b] Atomic layer deposition (ALD) was applied after measurements of emissivity and absorptivity of bare copper.

four disk-shaped samples (Fig. 2) was 40 mm in diameter and 1 mm in thickness. The discs were mechanically polished to a high gloss using a metallography polishing machine (typical surface characteristics after this process are $Ra = 0.01$ µm; $Rz = 0.05$ µm). We chose to use discs of this type, as they are compatible with the measurement apparatus used.

2.3. ALD coating

The ALD Al_2O_3 deposition was carried out with a Picosun R150 reactor using trimethylaluminum (TMA, $Al(CH_3)_3$) and deionized water at a temperature of 160 °C, with ~100 Pa reactor pressure. A piece of silicon wafer was included in each batch. Following the ALD process, the silicon wafer reference was measured with an ellipsometer (Semilab) to derive the thickness of the deposited ALD Al_2O_3 coating. The surface morphology of the ALD coating was investigated by a confocal microscope (Keyence) and a profilometer (Talystep). The data from the ellipsometer was verified by the profilometer measurement of the silicon reference sample having the highest ALD Al_2O_3 layer thickness (28.3 nm).

2.4. Laboratory measurements

The method for the measurement of emissivity and absorptivity is covered here. Our dedicated apparatus, along with the measuring method, has already been described thoroughly in our earlier paper [46]. The cylindrical measuring chamber with the sample is housed in a stainless-steel casing tube, immersed in an LHe bath inside a commercial LHe Dewar vessel. The vacuum is created by a turbomolecular pump before the cool down. During the measurement, a pressure lower than 10^{-7} Pa is maintained by cryogenic pumping with a sorbent in the casing tube.

We measure the radiative heat flow transferred between two

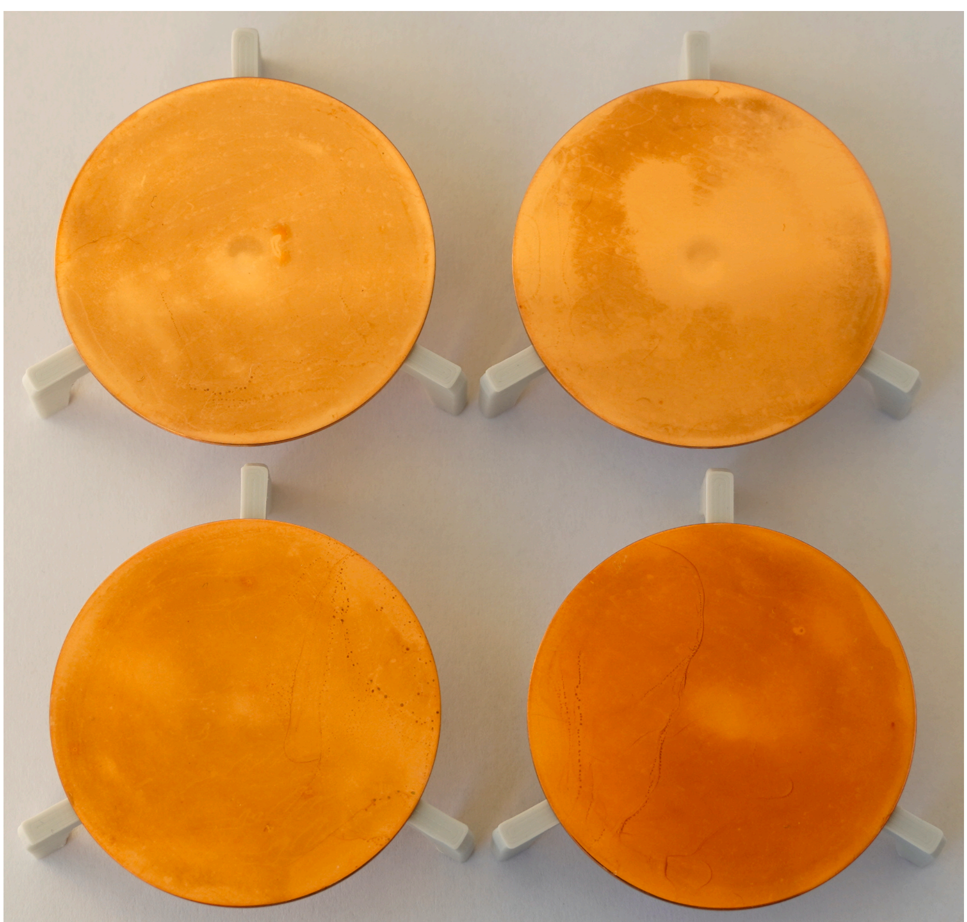

Fig. 2. Coated copper samples, each 40 mm in diameter, after the emissivity and absorptivity measurement. From upper left to lower right corner the samples numbered 01–04 with increasing layer thickness are shown.

concentric discs in the measuring chamber, a radiator (hot disk at temperature T_R) and an absorber (cold disk at temperature T_A), separated by a gap of about 0.5 mm. The examined sample is placed during emissivity measurement at the position of the radiator, while for absorptivity measurement the sample is in the position of the absorber. For both options, a "black" reference sample (an epoxy composite on a supporting copper disk with high absorptivity and emissivity of about 88%) is placed at the position opposite to the measured sample.

The radiator temperature T_R is gradually adjusted at selected setpoints from 20 K up to 320 K. A thermal resistor, acting as a heat flow meter (HFM), is made of a thin stainless-steel tube connecting the absorber (at T_A) with the HFM bottom flange (at $T_B = 5$ K). Transferred heat flows from the absorber through the heat flow meter to its bottom, from where it sinks into an LHe bath.

The total hemispherical emissivity or total hemispherical absorptivity of the sample is evaluated as a ratio between the measured heat power Q_R and the heat power $Q_B = A\sigma(T_R^4 - T_A^4)$ [W] that would be measured with 100%-absorbing samples (A denotes the sample area and σ the Stefan-Boltzmann [6] constant). The heat power Q_R can be calculated from the calibration curve of the HFM. This curve is obtained from the previous calibration process with a cold radiator when the absent radiative heat power on the absorber is simulated using the defined resistive heating on the absorber disk.

We use a Lake Shore 340 temperature controller for the measurement of T_R (using a Lake Shore DT470 SD silicon diode), T_A, T_B (both using Lake Shore Cernox™ CX 1050 sensors) and for setting and stabilization of T_R and T_B using resistive heaters. The expanded fractional uncertainty (coverage factor $k = 2$) in the case of emissivity or absorptivity measured on highly reflective samples is less than 11% of the value measured at $T_R \approx 30$ K, and less than 7% at temperatures above 60 K [46].

2.5. Computer-based analysis

By virtue of Kirchhoff's law, the emissivity of an opaque surface equals the absorptivity, $\varepsilon = \alpha = 1 - \rho$, at the same material temperature T_S, wavelength λ and direction θ (Fig. 1).

Using the infrared optical constants of Cu and Al_2O_3, we calculate the spectral directional reflectivity $\rho(\lambda, \theta, T_S)$ and absorptivity $\alpha(\lambda, \theta, T_S) = 1 - \rho(\lambda, \theta, T_S)$ of a smooth planar isotropic surface of copper covered with a thin Al_2O_3 layer (Fig. 3). Here T_S is the sample temperature. In accordance with Kirchhoff's law, the absorptivity $\alpha(\lambda, \theta, T_S)$ equals emissivity $\varepsilon(\lambda, \theta, T_S)$. Integrating over the hemisphere we obtain the spectral hemispherical absorptivity $\alpha(\lambda, T_S)$ and emissivity $\varepsilon(\lambda, T_S) = \alpha(\lambda, T_S)$, left panel in Fig. 4. The product of the absorptivity $\alpha(\lambda, \theta, T_S)$ and the spectral intensity of blackbody radiation at temperature T_R [7] integrated over wavelengths leads to the total directional absorptivity $\alpha(T_R, \theta, T_S)$ with respect to blackbody radiation (Fig. 4, right panel). Performing these two integrals over the directions and wavelengths, gives the total hemispherical absorptivity, $\alpha(T_R, T_S)$, which depends on both the sample temperature T_S and on the temperature T_R of the blackbody, and equals the total hemispherical emissivity $\alpha(T_R, T_R) = \varepsilon(T_R)$ for $T_S = T_R$ (Fig. 6, Table 2).

The analysis presented here is based on the optical constants of copper calculated using the Dingle approach to the anomalous skin effect [14] and using room temperature values of the complex index of refraction of hot-pressed alumina, tabularized in Palik's handbook [10]. We interpret and verify our calculations of the effect of the Al_2O_3 layer on emissivity/absorptivity by comparison with Berreman's approximation to this effect [16]. Finally, we justify the usage of room temperature optical constants of Al_2O_3 in the layer model at low temperatures.

2.5.1. Bare copper emissivity and absorptivity

We can see that the total hemispherical emissivity and absorptivity of a clean copper surface calculated using the Dingle formula for optical constants are weakly sensitive to copper's DC resistivity (Fig. 6). Here, the temperature dependence of DC resistivity is modelled for the defined residual resistivity $\rho_{res}(4\text{ K}) = \rho(300\text{ K})/RRR$, where RRR is a parameter known as the residual-resistivity ratio. The values $RRR = 6$ and $RRR = 100$ mean higher and lower DC resistivity (lower and higher purity of Cu), respectively. The curves in Fig. 6 give us a reasonable approximation for further analysis of the effect of the Al_2O_3 layer on copper emissivity. Further usage of $RRR = 100$ is based on a numerically tested and important fact, that the contribution of the Al_2O_3 layer to the calculated emissivity and absorptivity of copper is only slightly sensitive to the RRR value. The cause lies in the strong reflection of Cu

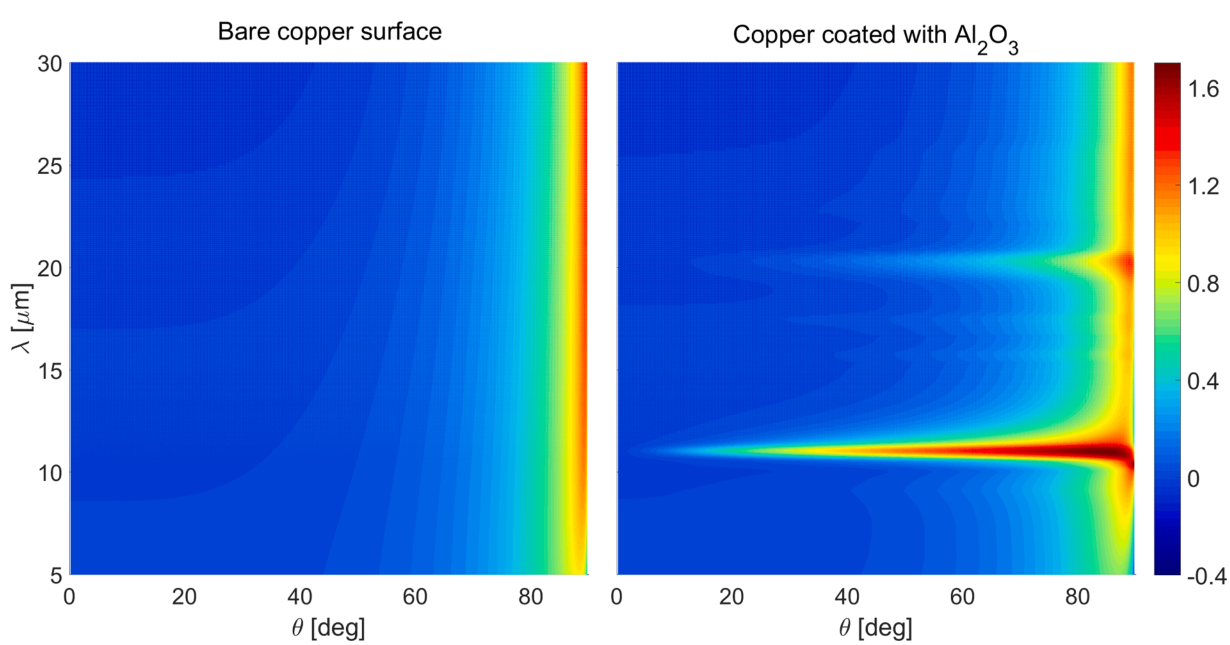

Fig. 3. Spectral directional absorptivity $\alpha(\lambda, \theta, T_S)$ of the clean copper surface (left plot) and the copper covered with a 28.3-nm thick alumina layer (right plot), both for the sample temperature $T_s = 300$ K. Absorptivity is plotted on the logarithmic scale in colours. Wavelengths are here limited to the interval where the absorption effect of Al_2O_3 is observed. The optical constants of hot-pressed alumina [10] were used.

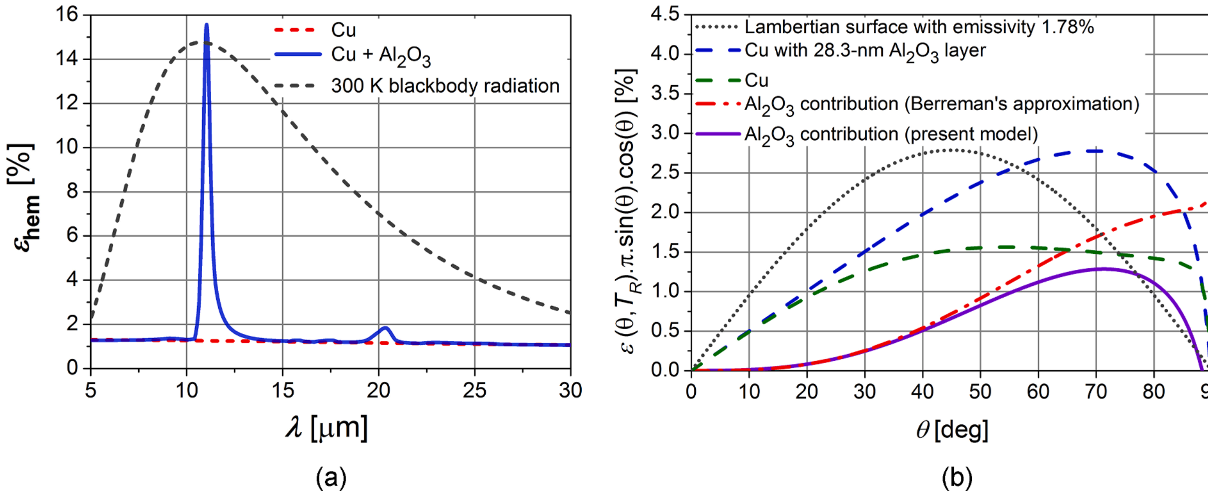

Fig. 4. Radiative properties of copper coated with a 28.3-nm thick layer of alumina calculated from the spectral directional absorptivity plotted in Fig. 3.
Left panel: Spectral hemispherical absorptivity/emissivity, $\alpha(\lambda, T_S) = \varepsilon(\lambda, T_S)$, $T_S = T_R = 300$ K. Spectrum of the blackbody radiation at temperature $T_R = 300$ K is plotted in arbitrary units.
Right panel: Angular (view angle) dependence of the total directional emissivity/absorptivity calculated for temperatures $T_S = T_R = 300$ K. Emissivity $\varepsilon(\theta, T_R) = \alpha(T_R, \theta, T_R)$ is multiplied with the function $\pi\sin(\theta)\cos(\theta)$, thus the total hemispherical emissivity is proportional to the area below a particular curve. The full line represents the contribution of Al_2O_3 to the emissivity of copper calculated in the numerical model as a difference between the values for Cu with and without the Al_2O_3 layer. The dash-dot line on the plot represents Berreman's approximation.

Table 2
Room-temperature total hemispherical emissivity of copper sample ($RRR = 100$) coated with a 28.3-nm thin layer of Al_2O_3 calculated using various data on the optical constants of Al_2O_3. The last two columns present the contribution of Al_2O_3 coating to the resulting emissivity.
Penultimate column: the differences between the numerical results in the 3rd column and the calculated emissivity 1.19% of clean copper at 300 K (Fig. 6).
Last column: Berreman's approximation of the Al_2O_3 contributions.

Al_2O_3 layer (28.3 nm) on Cu substrate (RRR = 100). $T = 300$ K, except for the last two rows.	Reference to data on optical constants.	Emissivity of coated Cu [%]	Contribution of coating to emissivity [%]	Contribution of coating to emissivity. Berreman's approx. [%]
Sapphire, ordinary ray	Gervais and Piriou [47]	1.85	0.66	1.01
Sapphire, ordinary ray	Palik, ed. [10]	1.93	0.73	0.86
Sapphire, extraordinary ray	Palik, ed. [10]	1.89	0.69	1.07
Alumina, hot-pressed	Palik, ed. [10] (Worrell, 1986)	1.78	0.59	0.86
Alumina 99.6%, SiO_2	Rajab et al. [48]	1.87	0.68	1.01
Alumina, sol-gel, annealed	Begemann et al. [49]	1.93	0.73	0.86
Alumina, evaporated	Eriksson et al. [50]	1.81	0.62	0.71
Clean Cu surface	Measured, **Fig. 7**	1.00	–	–
Al_2O_3, atomic layer deposition	Measured, **Figs. 7 and 8**	1.73	0.73	–
Clean Cu surface	Dingle [14]	1.19	–	–
Clean Cu surface, 77 K	Dingle [14]	0.56*)	–	–
Sapphire, ordinary ray, 77 K	Gervais and Piriou [47]	1.19*)	0.63**)	1.02

*Absorptivity.
**Contribution to absorptivity.

(reflectivity >98% in our case) because of the very high values of Cu permittivity.

2.5.2. *Copper with a thin layer of polar dielectric*

For a very thin layer of a polar dielectric on a metal with permittivity much higher than that of the dielectric, Berreman [16] derived an approximate formula for the directional spectral absorptivity (which equals spectral directional emissivity when we recall Kirchhoff's law) of such a system. Berreman verified this approximation with an experiment on reflection at the impact angle of about 30°. In Fig. 4 we compare the total directional emissivity calculated without any approximation, and the total directional emissivity based on Berreman's formula. We can see agreement between both angular dependences below the impact angle of about 40°. At higher angles, the Berreman approach fails, which is the reason for the difference between the total hemispherical values in the last two columns in Table 2 and between the heights of the main absorption peak in Fig. 5.

Nevertheless, Berreman's formula still gives a useful estimate of the effect of a thin layer on the total hemispherical emissivity, exceeding the values of more exact calculation for various Al_2O_3 materials by a modest margin of error (from 15% to about 50%, Table 2).

We tested the sensitivity of the emissivity to the Al_2O_3 structure. The effect of the Al_2O_3 layers on emissivity, calculated for a perfect sapphire crystal and alumina prepared via different technologies, varied within only 30% for the tested materials in Table 2.

We used the room-temperature optical constants of Al_2O_3 in the calculations of emissivity and absorptivity at all temperatures of the samples. A reasonably good agreement between experimental and theoretical results justifies this choice. Thus, from the experiment (see Results section), we can infer that the Al_2O_3 effect on emissivity does not depend strongly on the sample temperature. From a theoretical point of view, we can find a hint at explanation of this weak temperature dependence in Berreman's approximation of the dielectric function near the absorption peak (Eq. 14 in [16]). It is possible to show that, according to this approximate formula, the total emissivity depends only weakly on Al_2O_3 temperature. This is based on the assumption that "Berreman's" absorption peak is relatively narrow (Figs. 3 and 4) so that the intensity of the blackbody radiation and the damping term in dielectric function model would not change significantly over the peak's width. As a result of Berreman's formula and these assumptions, the

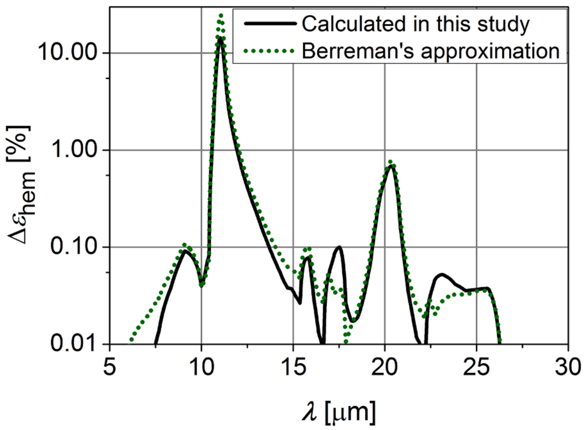

Fig. 5. Contribution of a 28.3-nm thin alumina layer to the spectral hemispherical emissivity of a copper substrate (difference between emissivities of Cu with and without ALD layer). The values at the highest peak are decisive for the total hemispherical emissivity. The complex permittivity (dielectric function) of hot-pressed alumina [10] was used in the numerical sample model and in Berreman's formula [16] (integrated here over hemisphere). Berreman's approximation is proportional to the imaginary part of the reciprocal dielectric function (energy loss function) given as $\mathrm{Im}(-1/\epsilon)$, where ϵ is permittivity. A logarithmic scale is used to see the spectra in all details.

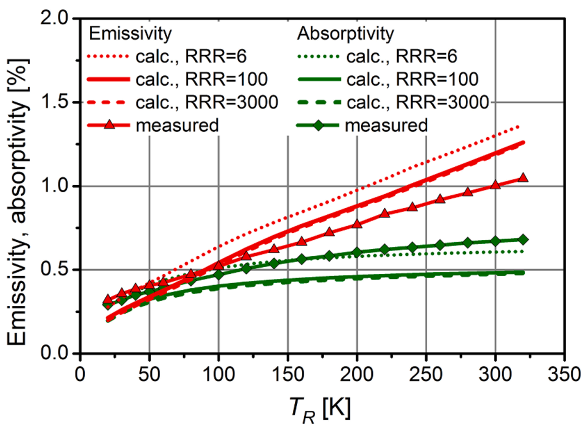

Fig. 6. Dependence of the total hemispherical emissivity and absorptivity of copper on the temperature of radiation. Values calculated within the ASE theory for low and high resistivity Cu ($RRR = 100$ and $RRR = 6$, respectively) in comparison with measured values for mechanically-polished technically pure copper. The temperature T_S of the sample in the absorptivity experiment and calculation is below 35 K for all values of T_R, specifically $T_S = 30$ K at $T_R = 300$ K. Note: Values of the emissivity and absorptivity calculated with $RRR = 3000$ (extremely pure Cu) nearly coincide with the values evaluated for $RRR = 100$.

total emissivity (integral over frequencies) does not depend on the damping term that could potentially cause the temperature dependence of the total emissivity. We performed another test of the temperature dependence using the optical constants of sapphire published for 77 K and 295 K [47] in calculations. Within this temperature interval, the contribution of Al_2O_3 to absorptivity and emissivity ($T_R = 300$ K, $T_S = 77$ K and $T_S = 300$ K) gives 0.63% and 0.66% in our model and 1.02% and 1.01% in Berreman's approximation, both proving weak temperature dependence.

2.5.3. Summary of analysis

To summarize, our analysis supports experimental results on the temperature and layer thickness dependence of the ALD Al_2O_3 layer effect on copper emissivity and absorptivity. In addition to the presented experiment, the computer-based analysis shows strong spectral selectivity of the effect, localized at wavelengths of about 11 μm (Fig. 3). We note that this absorption/emission peak is of parallel polarization, keeps its wavelength position with the change in angle, and varies its shape from a sharp shape in the sapphire and hot-pressed alumina (Fig. 3) to a broader and lower shape (not shown here) in dependence on the Al_2O_3 material type from Table 2.

3. Results

In the introduction, we discussed low-*e* solid surfaces with a particular focus on bulk copper. To investigate the possibility of retaining the inherent low emissivity of a copper substrate, despite an added passivating coating layer, we produced for our experiments four circular polished copper-disk samples with ALD Al_2O_3 layers deposited in various thickness (Fig. 2). The emissivity and absorptivity of each copper disk was measured before and after the ALD step, illustrated by the sequence of actions in Table 1. The emissivity values were measured at selected setpoints between 20 K and 320 K, while absorptivity measurements were limited up to 300 K.

During emissivity measurements (left column of subplots in Fig. 7) the sample itself is the source of thermal radiation (T_R), while in the case of absorptivity measurements (right column), the sample, kept at low temperature (T_S below 30 K), is irradiated with radiation of a blackbody at the temperature T_R (see Laboratory measurements in the Experimental details section). We can see that at a range of temperatures T_R, the absorptivity of clean copper is lower than its emissivity counterpart in Fig. 7, which reveals a temperature dependence of the optical properties of pure copper within the temperatures and infrared radiation relevant to our experiment.

A measurable increase in the copper emissivity and absorptivity, caused by the ALD Al_2O_3 coating, is observed above the temperature $T_R \approx 130$ K for the 4.5-nm thick layer and above $T_R \approx 80$ K for the 28.3-nm layer (Fig. 7).

This ALD Al_2O_3 contribution to the copper emissivity and absorptivity, calculated as a difference between the property measured with and without the layer, rises with the layer thickness and the temperature T_R (Fig. 8).

It is clear from Fig. 8 that there is a minor difference between the effect of ALD Al_2O_3 on emissivity and absorptivity, although the temperatures of the Al_2O_3 layer are up to one order of magnitude lower in the case of the absorptivity experiment. This indicates the weak dependence of the ALD Al_2O_3 effect on the temperature of the sample (on the Al_2O_3 temperature).

Theoretical values computed for the room temperature optical constants [10] of sapphire (Fig. 8) agree well with the experimental values presented here. Similar theoretical values are obtained for the optical properties published for several types of Al_2O_3 (Table 2). Computer-based analysis (see section Experimental details) shows the spectral and directional selectivity of the emission and absorption of thin layers of polar dielectrics, known as the Berreman effect. For smooth surfaces, strong absorption/emission of an Al_2O_3 thin layer at wavelengths of about 11 μm is expected in the oblique direction, while at directions near the normal angle of incidence the layers are transparent to infrared radiation.

In summary, we quantified the effect of a thin layer of ALD Al_2O_3, which contributed to copper emissivity and absorptivity. This contribution increases practically linearly with the Al_2O_3 layer thickness, increases with the temperature T_R of the radiation, and does not depend significantly on the temperature of the copper substrate from 30 K to 300 K. Experimental data agree well with the theoretical prediction when the optical constants of sapphire or hot-pressed alumina were used in the calculations.

4. Discussion

In the present work, the low-*e* nature of a polished copper surface is

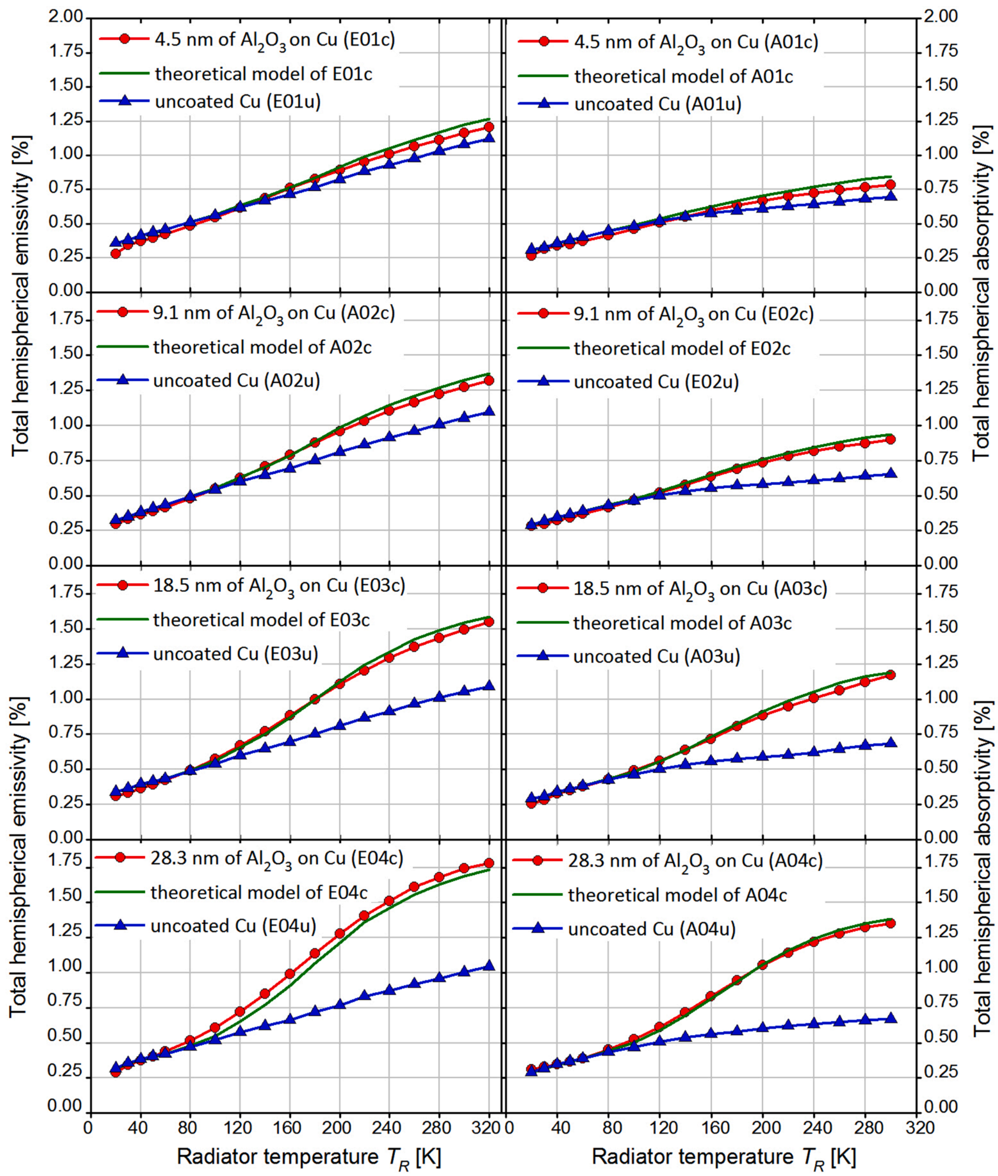

Fig. 7. Emissivity (left column) and absorptivity (right column) of copper-disk sample coated with ALD Al_2O_3 layer. The plot rows from top to bottom show the measurements of samples numbered 01–04 (Table 1) with increasing coating layer thickness from 4.5 to 28.3 nm (red lines with circles). Each plot contains the curve for a particular sample of bare copper before the deposition (blue lines with triangles). Theoretical values (green lines without symbols) were obtained by summation of the calculated contribution of a particular layer thickness to emissivity/absorptivity and the measured value of the uncoated copper surface.

considered as a fundamental technology, which can greatly benefit from having a protective ALD Al_2O_3 coating to passivate the surface. If oxidation and other chemical reactions on such copper surfaces can be prevented, the surface will retain its low thermal emittance. An ideal gas-barrier coating would prevent oxygen atoms (and other reagents) from reacting with the Cu atoms. However, almost any type of coating will inevitably increase the emittance of this surface, since properly polished copper has a lower value of thermal emittance compared to most other known materials from room temperature down to absolute zero [26].

The general scientific goal of this work was to investigate the effect of the selected coatings on the thermal radiative properties of polished copper discs from 20 K up to room temperature. Especially, the primary goal was to prove that a polished copper surface can be coated with a thin conformal ALD Al_2O_3 coating, while preserving the excellent low-*e* nature of such a surface.

In our previous work [51] which focused on the effects of thin gold layers, we used as the substrate very similar polished copper samples as those in this paper, having emissivity at room temperature of about 1%. By comparing the results, we can see that 28.3 nm of Al_2O_3 caused a similar increase in emissivity to about 1.8% as a 1–2 µm thick high-purity gold layer deposited by sputtering, the increase caused by the gold layer being even higher in the case of the electroplating (about 3.8%). Clearly, the results from this study deepen our understanding of how inorganic coatings, having thicknesses in the nanometer range, affect the thermal radiative properties of metals.

The selected coating (ALD) is chemically bonded to the substrate leading to good adhesion. It has been shown that for metal oxide films on metal substrates, an amorphous oxide film can be preferred over the crystalline state [42]. Both amorphous and crystalline ALD Al_2O_3 films have been shown to be excellent gas barriers [43,44]. The ALD recipe used in this study produces an amorphous Al_2O_3 film, which can effectively inhibit oxidation of the bulk Cu substrate. The thickness of such ALD Al_2O_3 films then becomes a critical factor, as our results clearly indicate (increase in emittance for increasing ALD coating thickness). It is difficult to give an exact optimum value for the coating thickness which is dependent on the intended usage scenario. The target thicknesses for this study were selected based on earlier work by Diaz et al. [45], where even a 10-nm ALD Al_2O_3 layer provided markedly improved corrosion resistance. Diaz also reported that the ALD Al_2O_3 layer should be thicker than 10 nm to seal the underlying substrate (carbon steel in their work) completely.

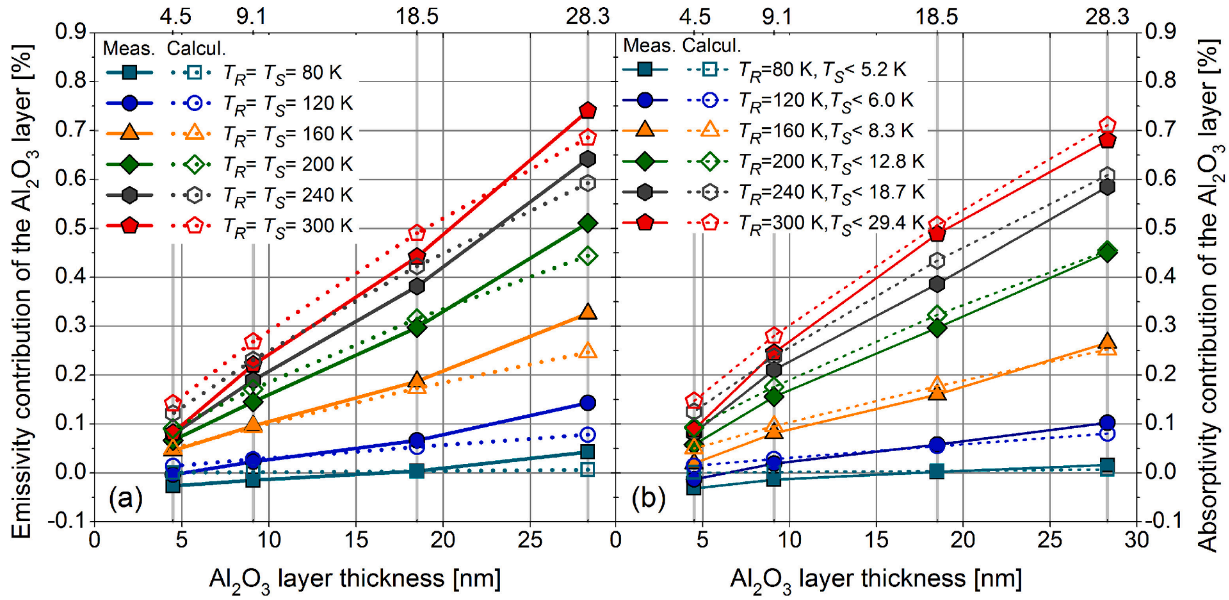

Fig. 8. Contribution of individual Al_2O_3 layers to the copper emissivity (left panel) and absorptivity (right panel), at various temperatures T_R of thermal radiation. The solid lines and filled symbols are for measured values, while dashed lines and opened symbols present the theoretical model. Each point for 4.5, 9.1, 18.5 and 28.3 nm in the plot was obtained as the difference between the emissivity or absorptivity value of the coated sample (measurements 01c, 02c, 03 or 04c) and of the uncoated sample (measured before coating in the runs 01u, 02u, 03u or 04u), respectively. The same procedure was applied to the theoretical values. T_S are the temperatures of the Al_2O_3 layer in the absorptivity measurements.

This ALD Al_2O_3 coating system may be of value in cryostat design, space technology and fusion reactors. For example, the ALD Al_2O_3 coating system could be combined with copper-clad steel to offer an alternative to the silver-coated steel thermal shields used in fusion reactors, the International Thermonuclear Experimental Reactor (ITER) being one such example. In cryostats, the ALD Al_2O_3 could offer an alternative to existing low-*e* coating systems for Cu, which have often relied on precious metals such as gold and silver [39]. In space technology, exposed copper has been mostly banned from spacecraft external surfaces, due to its susceptibility to atomic oxygen attack. However, the use of coated copper is not restricted. Related to this, NASA is currently researching several ALD coatings, including Al_2O_3, for future space missions [40]. Also, inorganic coatings have been shown to have good stability in the space environment [41]. The ALD Al_2O_3 coatings used in this study are so thin (< 30 nm) that problems associated with the well-known spacecraft surface charging phenomena are avoided. For spacecraft surface charging, voltage potentials exceeding 200 V are considered an issue [52,53]. The coatings used in this study are safe in this respect, because estimation based on the dielectric strength of 13.4 AC-MV/m [54] and a 28 $\times$ 10^{-9} m thick Al_2O_3 layer indicates that they are not able to sustain voltage potentials higher than about 0.4 V (= 13.4 $\times$ 10^6 V/m $\times$ 28 $\times$ 10^{-9} m). Finally, as the post-JWST telescopes are expected to have increased demands to reach ultra-low mirror and sensor temperatures, ALD Al_2O_3-protected Cu could be considered as a candidate for constructing their sunshields, as a thin ALD Al_2O_3 film is also well-suited for surfaces containing bends.

5. Conclusions

The effect of a thin-film ALD Al_2O_3 coating on the radiative properties of polished copper was measured from 20 K up to room temperature. This study included four Al_2O_3 layer thicknesses (4.5, 9.1, 18.5 and 28.3 nm). The applied computational model of the Al_2O_3 coating effect on emissivity and absorptivity is in reasonable agreement with experimental results. Our analysis provides details on spectral, directional and temperature dependencies, better enabling the prediction and understanding of the effect of a thin layer of ALD Al_2O_3 on thermal emissivity and absorptivity of highly reflective metallic surfaces.

Our results show that polished copper can be coated with a passivating ALD Al_2O_3 thin-film barrier coating, while largely preserving the inherent low thermal emissivity of copper.

The use of ALD Al_2O_3 is a pathway for the development of a practical and inexpensive low-*e* coating system for copper. This type of coating may be applied in various fields, including cryostat design, space technology and fusion reactors.

Data availability

The data that support the findings of this study are available from the corresponding author upon request.

CRediT authorship contribution statement

Leo Nyman: Conceptualization, Methodology, Supervision, Writing – original draft. **Jiří Frolec:** Methodology, Investigation, Supervision, Writing – original draft. **Marko Pudas:** Conceptualization, Resources. **Tomáš Králík:** Investigation, Validation, Visualization. **Věra Musilová:** Methodology, Validation, Formal analysis, Visualization. **Esa Kallio:** Supervision.

Declaration of Competing Interest

The authors declare no competing interests.

Acknowledgements

We thank Dr. Antti Kestilä at the Finnish Meteorological Institute for discussions on space mission aspects. This work was supported by MEYS CR, EC, and CAS (LO1212, CZ.1.05/2.1.00/01.0017, RVO:68081731).

References

[1] J.G. Weisend, Principles of Cryostat Design, Cryostat DesignSpringer, Cham, 2016, pp. 1–45.
[2] S. Orlandi, ITER Project: International Cooperation and Energy Investment. In International Cooperation for Enhancing Nuclear Safety, Security, Safeguards and Non-proliferation, Springer, Cham, 2020, pp. 169–191.

[3] F. Sabourin, J.M. Martinez, N. Gupta, J.B. Layly, D. Patel, J. Chenard, S.P. Singh, T. Arzoumanian, G.P. Pichel, N.I. Her, C.H. Choi, Application of 3D view factor method for heat fluxes deposition on ITER cryostat thermal shield, Fusion Eng. Des. 138 (2019) 239–246.
[4] S.I. Woods, T.M. Jung, D.R. Sears, J. Yu, Emissivity of silver and stainless steel from 80 K to 300 K: application to ITER thermal shields, Cryogenics (Guildf) 60 (2014) 44–48.
[5] V. Musilova, T. Kralik, P. Hanzelka, A. Srnka, Effect of different treatments of copper surface on its total hemispherical absorptivity bellow 77 K, Cryogenics (Guildf) 47 (4) (2007) 257–261.
[6] L. Boltzmann, Ueber eine von Hrn. Bartoli entdeckte Beziehung der Wärmestrahlung zum zweiten Hauptsatze, Ann Phys. 258. 5 (1884) 31–39.
[7] J.R. Howell, M.P. Mengüc, K. Daun, R. Siegel, Thermal Radiation Heat Transfer, CRC Press, Boca Raton, 2020.
[8] E. Hagen, H. Rubens, Über Beziehungen des Reflexions- und Emissionsvermögens der Metalle zu ihrem elektrischen Leitvermögen, Ann. Phys. 316 (8) (1903) 873–901.
[9] P. Drude, Zur elektronentheorie der metalle, Ann. Phys. 306 (3) (1900) 566–613.
[10] E.D. Palik, Handbook of Optical Constants of Solids, Vol. 2, Academic Press, 1998.
[11] G.E.H. Reuter, E.H. Sondheimer, The theory of the anomalous skin effect in metals, Proc. R. Soc. Lond. A 195 (1948) 336–364.
[12] M.I. Kaganov, G. Ya Lyubarskiy, A.G. Mitina, The theory and history of the anomalous skin effect in normal metals, Phys. Rep. 288 (1–6) (1997) 291–304.
[13] G.A. Domoto, R.F. Boehm, C.L. Tien, Predictions of the total emissivity of metals at cryogenic temperatures, Adv. Cryogenic Eng 14 (1969) 230–239.
[14] R.B. Dingle, The anomalous skin effect and the reflectivity of metals I, Physica 19 (1–12) (1953) 311–347.
[15] V. Musilova, P. Hanzelka, T. Kralik, A. Srnka, Low temperature radiative properties of materials used in cryogenics, Cryogenics (Guildf) 45 (2005) 529–536.
[16] D.W. Berreman, Infrared absorption at longitudinal optic frequency in cubic crystal films, Phys. Rev. 130 (6) (1963) 2193–2198.
[17] C. Kittel, Introduction to Solid State Physics, 8th ed., Willey, 2004.
[18] P. Grosse, V. Offermann, Quantitative infrared spectroscopy of thin solid and liquid films under attenuated total reflection conditions, Vib. Spectrosc. 8 (1995) 123–133.
[19] S. Vassanti, J.P. Hugonin, F. Marquier, J.J. Greffet, Berreman mode and epsilon near zero mode, Opt. Express 20 (2012) 23971–23977.
[20] N. Nordin, O. Dominguez, C.M. Roberts, W. Streyer, K. Feng, Z. Fang, V. A. Podolskiy, A.J. Hoffman, D. Wasserman, Mid-infrared epsilon-near-zero modes in ultra-thin phononic films, Appl. Phys. Lett. 111 (2017), 091105.
[21] M. Hieta, M. Genzer, H. Haukka, A. Kestilä, I. Arruego, V. Apéstigue, J. Martínez, M. Reina, C. Ortega, C. Camañes, I. Sard, MiniPINS-miniature in situ sensor packages for mars and moon, in: European Planetary Science Congress, September 2020. EPSC2020-858.
[22] J. Arenberg, J. Flynn, A. Cohen, R. Lynch, J. Cooper, Status of the JWST sunshield and spacecraft, in: Proc. SPIE 9904, Space Telescopes and Instrumentation 2016: Optical, Infrared, and Millimeter Wave, 9 August 2016, 990405, https://doi.org/10.1117/12.2234481.
[23] James Webb space telescope, the sunshield. https://www.jwst.nasa.gov/content/observatory/sunshield.html, 2021 (accessed 22 April 2021).
[24] A.C. Phillips, J. Miller, W. Brown, D. Hilyard, B. Dupraw, V. Wallace, D. Cowley, Progress toward high-performance reflective and anti-reflection coatings for astronomical optics, in: Advanced Optical and Mechanical Technologies in Telescopes and Instrumentation, 7018, International Society for Optics and Photonics, July 2008, p. 70185A, https://doi.org/10.1117/12.789862.
[25] E.A. Estalote, K.G. Ramanathan, Low-temperature emissivities of copper and aluminum, J. Opt. Soc. Am. 67 (1) (1977) 39–44.
[26] J. Frolec, T. Králík, V. Musilová, P. Hanzelka, A. Srnka, J. Jelínek, A database of metallic materials emissivities and absorptivities for cryogenics, Cryogenics (Guildf) (97) (2019) 85–99.
[27] Y. Unutulmazsoy, C. Cancellieri, M. Chiodi, S. Siol, L. Lin, L.P. Jeurgens, In situ oxidation studies of Cu thin films: growth kinetics and oxide phase evolution, J. Appl. Phys. 127 (6) (2020), 065101.
[28] K. Fujita, D. Ando, M. Uchikoshi, K. Mimura, M. Isshiki, New model for low-temperature oxidation of copper single crystal, Appl. Surf. Sci. 276 (2013) 347–358.
[29] D.L. Cocke, R. Schennach, M.A. Hossain, D.E. Mencer, H. McWhinney, J.R. Parga, M. Kesmez, J.A.G. Gomes, M.Y.A. Mollah, The low-temperature thermal oxidation of copper, Cu3O2, and its influence on past and future studies, Vacuum 79 (1–2) (2005) 71–83.
[30] G.N. Raikar, J.C. Gregory, P.N. Peters, Oxidation of copper by fast atomic oxygen, Oxidation of Metals 42 (1–2) (1994) 1–15.
[31] ECSS (European Coordination for Space Standardization). "European coordination for space standardization." https://www.ecss.nl, 2021 (accessed 25 April 2021).
[32] T. Suntola, J. Antson. Method for producing compound thin films. U.S. Patent 4,058,430, filed November 25, 1975 and issued November 15, 1977.
[33] T. Kutilainen, M. Pudas, M.A. Ashworth, T. Lehto, L. Wu, G.D. Wilcox, J. Wang, P. Collander, J. Hokka, Atomic layer deposition (ALD) to mitigate tin whisker growth and corrosion issues on printed circuit board assemblies, J. Electron. Mater. 48 (11) (2019) 7573–7584.
[34] M. Broas. Quality, microstructural refinement and stability of atomic-layer-deposited aluminum nitride and aluminum oxide films. (2018).
[35] M.L. Chang, T.C. Cheng, M.C. Lin, H.C. Lin, M.J. Chen, Improvement of oxidation resistance of copper by atomic layer deposition, Appl. Surf. Sci. 258 (24) (2012) 10128–10134.
[36] A.I. Abdulagatov, Y. Yan, J.R. Cooper, Y. Zhang, Z.M. Gibbs, A.S. Cavanagh, R. G. Yang, Y.C. Lee, S.M. George, Al2O3 and TiO2 atomic layer deposition on copper for water corrosion resistance, ACS Appl. Mater. Interfaces 3 (12) (2011) 4593–4601.
[37] J. Charlier, Vacuum deposited optical coatings experiment, in: LDEF, 69 months in space: first post-retrieval symposium Vol. 3134, 1991, p. 1343.
[38] I.N. Reddy, A. Dey, N. Sridhara, S. Anoop, P. Bera, R.U. Rani, C. Anandan, A. K. Sharma, Corrosion behaviour of sputtered alumina thin films, J. Institution of Engineers (India): Series D 96 (2) (2015) 105–112.
[39] P. Micke, J. Stark, S.A. King, T. Leopold, T. Pfeifer, L. Schmoeger, M. Schwarz, L. J. Spieß, P.O. Schmidt, J.R. Crespo López-Urrutia, Closed-cycle, low-vibration 4 K cryostat for ion traps and other applications, Rev. Sci. Instrum. 90 (6) (2019), 065104.
[40] D. Butler, T. Swanson, NASA Goddard thermal technology overview, 2017.
[41] M. Hołyńska, A. Tighe, C. Semprimoschnig, Coatings and Thin Films for Spacecraft Thermo-Optical and Related Functional Applications, Adv Mater Interfaces 5 (11) (2018), 1701644.
[42] L.P.H. Jeurgens, W.G. Sloof, F.D. Tichelaar, E.J. Mittemeijer, Thermodynamic stability of amorphous oxide films on metals: application to aluminum oxide films on aluminum substrates, Phys. Rev. B 62 (7) (2000) 4707.
[43] M. Broas, J. Lemettinen, T. Sajavaara, M. Tilli, V. Vuorinen, S. Suihkonen, M. Paulasto-Kröckel, In-situ annealing characterization of atomic-layer-deposited Al2O3 in N2, H2 and vacuum atmospheres, Thin Solid Films 682 (2019) 147–155.
[44] D.S.B. Heidary, W. Qu, C.A. Randall, Evaluating the merit of ALD coating as a barrier against hydrogen degradation in capacitor components, RSC Adv 5 (63) (2015) 50869–50877.
[45] B. Díaz, E. Härkönen, J. Światowska, V. Maurice, A. Seyeux, P. Marcus, M. Ritala, Low-temperature atomic layer deposition of Al2O3 thin coatings for corrosion protection of steel: surface and electrochemical analysis, Corrosion Sci 53 (6) (2011) 2168–2175.
[46] T. Kralik, V. Musilova, P. Hanzelka, J. Frolec, Method for measurement of emissivity and absorptivity of highly reflective surfaces from 20 K to room temperatures, Metrologia 53 (2) (2016) 743, https://doi.org/10.1088/0026-1394/53/2/743.
[47] F. Gervais, B. Piriou, Anharmonicity in several-polar-mode crystals: adjusting phonon self-energy of LO and TO modes in Al2O3 and TiO2 to fit infrared reflectivity, J. Phys. C: Solid State Physics 7 (1974) 2374–2386.
[48] K.Z. Rajab, M. Naftaly, E.H. Linfield, J.C. Nino, D. Arenas, D. Tanner, R. Mittra, M. Lanagan, Broadband dielectric characterization of aluminum oxide (Al2O3), Journal of Microelectronics and Electronic Packaging 5 (1) (2008) 2–7.
[49] B. Begemann, J. Dorschner, T. Henning, H. Mutschke, J. Guertler, C. Koempe, R. Nass, Aluminum oxide and the opacity of oxygen-rich circumstellar dust in the 12–17 μm range, Astrophys. J. 476 (1) (1997) 199.
[50] T.S. Eriksson, A. Hjortsberg, G.A. Niklasson, C.G. Granqvist, Infrared optical properties of evaporated alumina films, Appl. Optic. 20 (15) (1981) 2742–2746.
[51] J. Frolec, T. Králík, A. Srnka, Low temperature thermal radiative properties of gold coated metals, Int. J. Refrigeration 82 (2017) 51–55.
[52] D. Hastings, H. Garrett, Spacecraft-environment Interactions, Cambridge University Press, 2004.
[53] H. Garrett, A. Whittlesey, Spacecraft charging, an update, IEEE Trans. Plasma Sci. 28 (6) (2000) 2017–2028.
[54] W.M. Haynes (Ed.), CRC Handbook of Chemistry and Physics, CRC Press, 2014.